Journal of
Synchrotron Radiation

ISSN 0909-0495

Received 28 August 2007
Accepted 21 November 2007

Dedicated to the memory of the late Harold Eastgate

Migration of mercury from dental amalgam through human teeth

Hugh H. Harris,[a]*‡ Stefan Vogt,[b] Harold Eastgate,[c] Daniel G. Legnini,[b] Benjamin Hornberger,[d] Zhonghou Cai,[b] Barry Lai[b] and Peter A. Lay[a]*

[a]School of Chemistry, The University of Sydney, NSW 2006, Australia, [b]X-ray Science Division, Argonne National Laboratory, Argonne, IL 60439, USA, [c]Eastmac Pty Ltd, 8 Cassinia Close, Knoxfield, VIC 3180, Australia, and [d]Department of Physics and Astronomy, Stony Brook University, Stony Brook, NY 11794, USA. E-mail: hugh.harris@adelaide.edu.au, p.lay@chem.usyd.edu.au

Exposure to mercury from dental amalgams, with possible negative health effects, has generally been considered to occur *via* either erosion or evaporation directly from the surface of fillings, followed by ingestion. The aim of this study was to determine the relative importance of the direct migration of mercury through the tooth as an alternative exposure pathway. X-ray fluorescence imaging has been used to determine quantitatively the spatial distribution of Hg, Ca, Zn and Cu in sections of human teeth that had been filled with amalgam for more than 20 years. X-ray absorption near-edge spectroscopy (XANES) was also employed to gain chemical information on the mercury present in the teeth. Hg (up to $\sim$10 mg g^{-1}) and Zn (>100 mg g^{-1}) were detected in the teeth several millimetres from the location of the amalgams. At high resolution, Hg showed higher concentrations in dentinal tubules while Zn was generally evenly distributed. XANES showed that the chemical form of Hg that had migrated into the tooth had been altered from that present in the amalgam. The differing spatial distributions of Hg and Zn suggest distinct transport mechanisms for the two metals, presumably chemical for Zn and initially physical for Hg. Subsequent oxidation of Hg may lead to a loss of mobility or the development of a secondary transport mechanism. Most importantly the detection of Hg in areas of the tooth that once contained an active bloodstream and in calculus indicates that both exposure pathways should be considered as significant.

Keywords: amalgam; dental restoration; mercury toxicity; X-ray fluorescence imaging; human teeth.

1. Introduction

The issue of the toxicity and long-term side effects of dental amalgam fillings remains contentious. The more conservative view, that the benefits of amalgam fillings outweigh possible health concerns, is generally better respected in the scientific literature (Clarkson *et al.*, 2003) and recent comprehensive epidemiological studies suggest that links between the use of dental amalgam and a number of implicated conditions are weak at most (Kingman *et al.*, 2005; Bates *et al.*, 2004). However, anecdotal evidence for such links is abundant and 'dissident' dentists have developed new techniques for safer removal of amalgam fillings owing to demand from patients. Meanwhile, in 1997, an estimated 40 metric tons of mercury was used in dental restorations in the USA (Reese Jr, 1997). For perspective, the annual figure for industrially sourced mercury pollution deposited in the USA in 1997 was estimated at 52 metric tons (EPA, 1997).

The fact that the presence of amalgam fillings leads to increased levels of Hg in various organs in the body, such as blood and kidney, as well as in urine is unquestioned (Kingman *et al.*, 1998; Sallsten *et al.*, 1996), but argument continues as to whether these levels are deleterious to human health. With one exception (Hoffmann *et al.*, 2000), studies of amalgam toxicity have assumed that the only significant pathway of exposure to be *via* ingestion or inhalation of elemental Hg from the surface of fillings. However, exposure *via* migration of mercury through the tooth and into the active bloodstream of the pulp, and/or by concentration in the calculus, may considerably confound epidemiological results. We have performed an initial study using X-ray microprobe techniques on extracted amalgam-filled teeth in an effort to determine the significance of these pathways and, owing to the greatly varying toxicity of different chemical forms of mercury,

‡ Present address: School of Chemistry and Physics, The University of Adelaide, SA 5005, Australia.

the type of mercury entering the bloodstream through the tooth.

2. Experimental

2.1. Tooth sample preparation

Suitable extracted teeth were collected in Melbourne, Australia (Knox Dental Group, Wantirna Sth, Victoria). Tooth donors signed release forms permitting the use of teeth for experimental purposes, along with the release of their medical histories. Teeth extracted were of two types: restored with amalgam only, and control teeth extracted for orthodontic reasons that had no previous restorations. Teeth were stored in formalin after extraction. Amalgam fillings and linings were removed after extraction with a high-speed dental drill. Linings were not unambiguously identified but, based on the age of the fillings (dental records did not allow exact aging of restorations, recollections of patients as well as the visual appearance of the amalgams indicated that they were at least 20–40 years old), were most likely to consist of either ZnO- or $Zn_3(PO_4)_2$-based materials, still in common usage today. The teeth were then horizontally sectioned to 100 μm (minimum self-supporting thickness) using a diamond saw (circular diamond blade, 10 cm diameter, manufactured by Universal Grinding Wheel Co., Stansford, UK) cutting through the site of the removed filling last to minimize the possibility of contamination of the section surface by residual amalgam. Sections were then mounted on aluminium posts for analysis. Each section illustrated in the figures originated from a different tooth.

2.2. X-ray fluorescence microprobe imaging

The X-ray fluorescence (XRF) scanning microprobe technique used in this study allows the simultaneous and accurate determination of the two-dimensional spatial distribution of elements (ranging in atomic mass from P upwards) in a sample of interest, with sensitivity as high as the attogram range for heavier elements. The technique has been described in detail elsewhere (Ilinski *et al.*, 2003). XRF data collection was performed on the 2-ID-E beamline at the Advanced Photon Source, Argonne National Laboratory, IL, USA.

Elemental distribution maps were collected at room temperature under a He atmosphere, using a 13.4 keV monochromatic X-ray incident beam, and one of the following beam-defining or focusing devices: a 100 μm pinhole for coarse elemental maps; and a single zone plate and order-sorting aperture device generating a 1 μm × 0.5 μm spot for fine elemental maps (Yun *et al.*, 1999). The fluorescence signal was detected at 90° to the incident beam using a three-element solid-state Ultra LEGe detector (Canberra). The incident beam struck at 30° away from the normal of the face of the teeth sections to allow efficient escape of the fluorescent signal. Quantitation (elemental area densities in μg cm^{-2}) was performed using *MAPS* software (Vogt, 2003), by fitting the full fluorescence spectrum at every single point to modified Gaussians (Van Espen, 2002) and comparing with corresponding measurements on the thin-film standards NBS-1832 and NBS-1833 from the National Bureau of Standards (NBS/NIST, Gaithersburg, MD, USA). These values were converted to mg g^{-1} assuming a density for the sample of 2.1 g cm^{-3} (Coklica *et al.*, 1969) and a section thickness of 100 μm. A correction for re-absorption of the fluorescence signal from each element of interest by the hydroxyapatite matrix was made by performing a numerical integration (100 nm steps) of the absorption through 200 μm of sample (assuming that the average angle of escape of fluorescent photons is 60° from the face of the section, and the fluorescing element is distributed evenly throughout the thickness of the sample) and assuming the sample was pure hydroxyapatite with a density of 2.1 g cm^{-3}.

Differential phase-contrast (DPC) images were also collected at beamline 2-ID-E. These images emphasize discontinuities in the structures of samples consisting of mainly lighter elements such as Ca and P that would be difficult to detect using standard transmission techniques. The technique has been described in detail elsewhere (Feser *et al.*, 2003; Vogt *et al.*, 2004). XANES spectra were collected at beamline 2-ID-D at the APS, using a dual zone plate and order-sorting aperture generating a 0.2 μm × 0.2 μm spot, a single-element solid-state Ge detector, and a double-crystal Si(111) monochromator. The spectra were collected over a 100 eV range with 0.5 eV steps and a 1 s count time per point. The spectra were energy calibrated to the first inflexion point of elemental Hg (at 12284.0 eV) assuming that the spectrum of the residual amalgam (see below) was identical to elemental Hg.

3. Results

Fig. 1 shows 100 μm resolution XRF elemental distribution maps for two 100 μm-thick horizontal sections of molar teeth that had been filled with amalgam for more than 20 years, along with corresponding optical micrographs. A schematic for the class 2 cavities originally present in these teeth is shown in the supplementary material.[1] The calcium maps for both samples are unsuprisingly uniform across the sections with somewhat higher intensities corresponding to the enamel, where the hydroxyapatite content is the highest, and lower intensities corresponding to the pulp region. Notably, locally high levels of Zn are observed, corresponding to the brown-stained region of the teeth, adjacent to the fillings. In the same region, but with intensities one to two orders of magnitude lower than that for Zn, are localizations of Hg. Significant quantities of Hg are also detected in the region of accumulated calculus in the optical micrograph on the right-hand edge of both sections shown in Fig. 1. The possibility that this signal arises from increased escape efficiency of fluorescent photons through the side of the tooth is primarily eliminated on the basis that, during the experiment, the fluorescence detector

[1] Supplementary data for this paper are available from the IUCr electronic archives (Reference: HI5582). Services for accessing these data are described at the back of the journal.

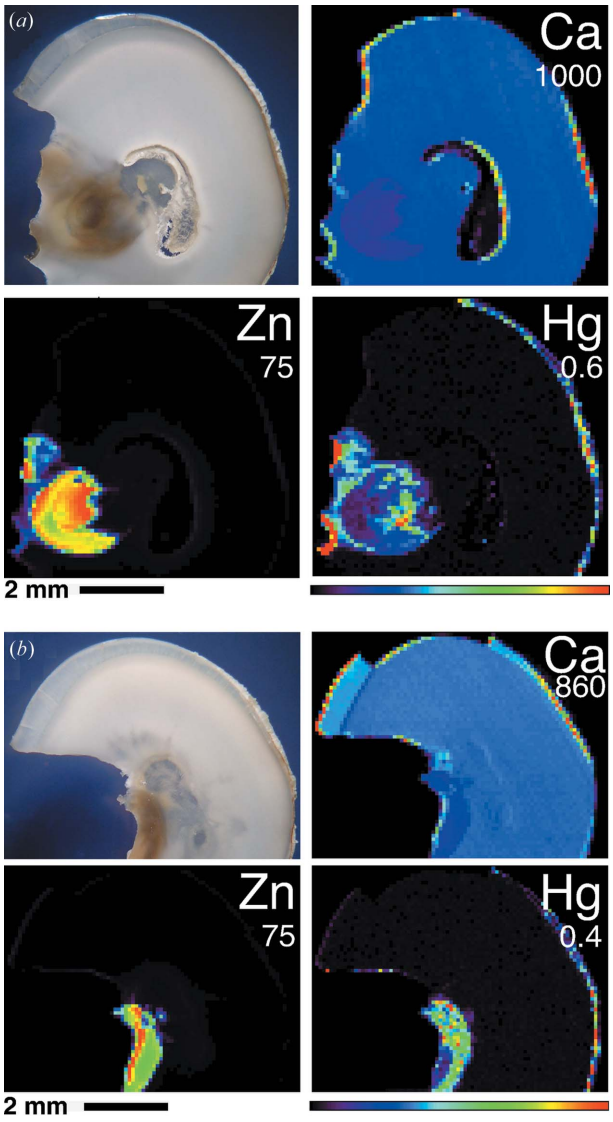

Figure 1
Optical micrographs [top left of (*a*) and (*b*)] and XRF (100 µm resolution) elemental distribution maps for 100 µm-thick horizontal sections of two human teeth filled with amalgam for >20 years. The site of the fillings is on the left side of each tooth. It is noted that some of the enamel from the top of each tooth was lost prior to XRF imaging. Maxima for each element in mg g^{-1} (assuming a density of 2.1 g cm^{-3}) are given below the element symbol.

was placed on the opposite side of the tooth to the high Hg edge. It is noted that the areas of the brown stains and the corresponding regions of high Zn and Hg stretch from the location of the filling to the boundary of the dentine and the pulp, as identified in the optical micrographs. Both sections pictured in Fig. 1 show transparent areas at the centre that have corresponding high intensities in the Ca maps, indicating the presence of secondary dentine that has replaced pulp over time. An area of residual pulp is indicated in the low-intensity crescent-shaped area in the Ca map in Fig. 1(*a*).

It is noted that the migration of the metals is not consistent across the filling/dentine boundary. In both samples there were regions of dentine that should have been in direct contact with amalgam that showed no significant levels of either Zn or Hg.

Examination of unfilled control teeth (not shown), extracted from teenagers for orthodontic reasons, revealed that levels of Zn (<0.1 mg g^{-1}) and Hg (<5 µg g^{-1}) were below the measured background.

Fig. 2 shows a much higher resolution scan (1.5 µm) of a portion of dentine directly adjacent to the removed class 2 amalgam filling of a molar tooth. Again, as expected, Ca is evenly distributed throughout the sample, and the Zn map also shows a very even distribution. In contrast, two small bright spots are observed in the same position in the Hg and Cu maps, on the dentine/filling boundary. The DPC image of the same region of tooth also shows points on the boundary corresponding to the Hg and Cu hotspots. The high concentrations of Hg and Cu in these bright spots, along with evidence for the presence of Ag in the XRF spectrum (data not shown), strongly implies that these are residual pieces of amalgam that escaped the dental drilling process or diffused through cracks in the teeth.

Also noted in the DPC image are almost horizontal striations roughly 3 µm wide that, based on width, density and direction, were assumed to be dentinal tubules (Berkovitz *et al.*, 1992). The possibility that these striations are saw cut marks was eliminated on the basis that the saw direction would have left striations roughly perpendicular to what was observed. We observe some correspondence between the striations in the DPC image and regions of high intensity of Hg in Fig. 2. This correspondence is confirmed in Fig. 3, which shows a 0.5 µm resolution scan of the area marked by a red box in Fig. 2. Again, in Fig. 3, we observe a co-localization of Cu and Hg in areas identified as tubules from the DPC image and that, in contrast, Ca and Zn have similar and very even distributions.

Hg L_{III}-edge XANES spectra of the residual amalgam and of the Hg present in tubules are presented in Fig. 2. A significant variation is noted between these spectra and, while they are not of sufficient quality to provide unambiguous Hg speciation, it is clear that the Hg present in the tubules has undergone at least partial oxidation with respect to that in the residual amalgam.

Fig. 4 shows elemental distribution maps for Ca and Hg of a 50 µm × 50 µm region of tooth section shown by the red arrow in Fig. 2. The presence of the observed Hg hotspot, in a region of low Ca intensity, was initially somewhat surprising at such a distance from the site of the filling. The presence of a class 2 filling in this tooth that also covers much of the tooth crown, and the fact that the tooth had been sectioned just below this part of the filling, provides a feasible source for the hotspot in terms of an extension of a filament of the pulp into the region of the dental filling (see supplementary material). Also shown in Fig. 4 is the XRF spectrum for the Hg hotspot, indicating that this is a particularly Hg-rich fragment of amalgam.

We note that the maximum concentrations shown in the figures for Zn, and in particular Ca, are not physically reasonable (*i.e.* >1000 mg g^{-1}) and we suggest two sources of error that may produce these values. Firstly, the periphery of

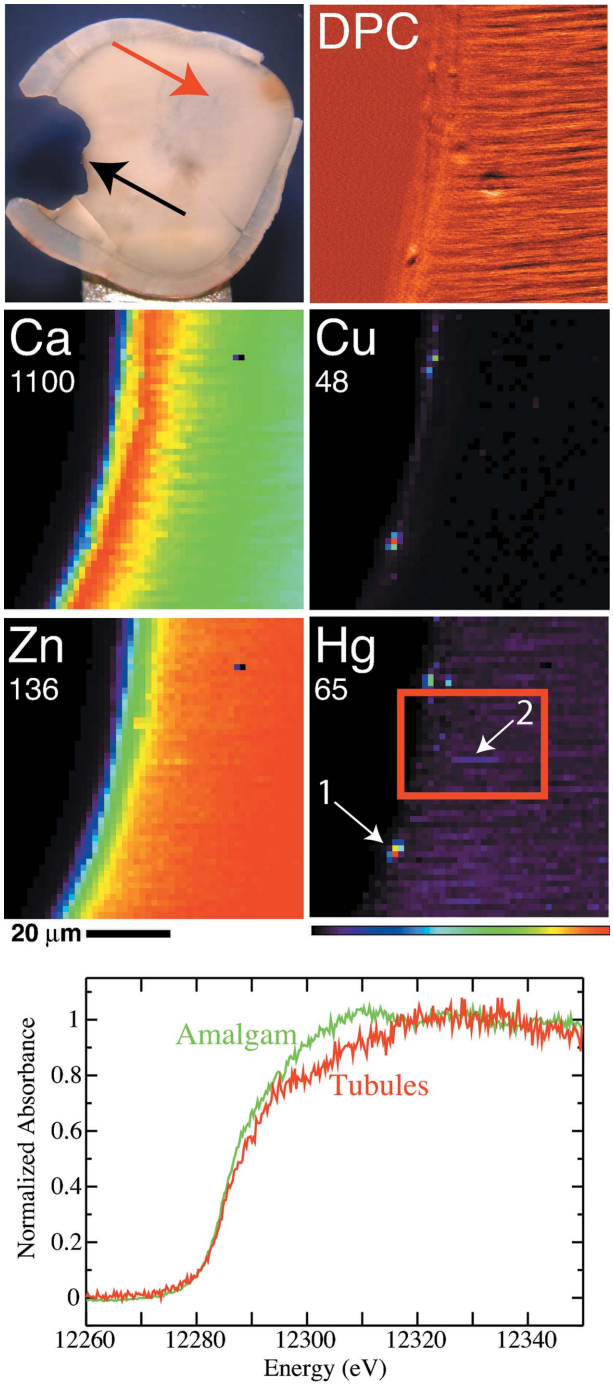

Figure 2
Top: optical micrograph (top left), X-ray differential phase contrast (DPC, top right) and XRF (1.5 μm resolution) elemental distribution maps for a 100 μm-thick section of a human tooth filled with amalgam for >20 years. The site of the filling is on the left side of the tooth. The scan region (75 μm × 75 μm) for the DPC and XRF images is indicated by the black arrow in the optical micrograph. The scale bar only applies to the XRF and DPC images; the scale for the optical micrograph is similar to that of Fig. 1. Maxima for each element in mg g^{-1} (assuming a tooth density of 2.1 g cm^{-3}) are given below the element symbol. The red box and red arrow indicate the location of finer scans displayed in Figs. 3 and 4. Points 1 and 2 indicate the location for XANES spectra shown at the bottom of the figure. Bottom: Hg L_{III}-edge XANES spectra from 0.25 μm × 0.25 μm spots as indicated in the Hg map. The trace in green corresponds to residual amalgam (point 1) while the red trace corresponds to the Hg present in tubules (point 2).

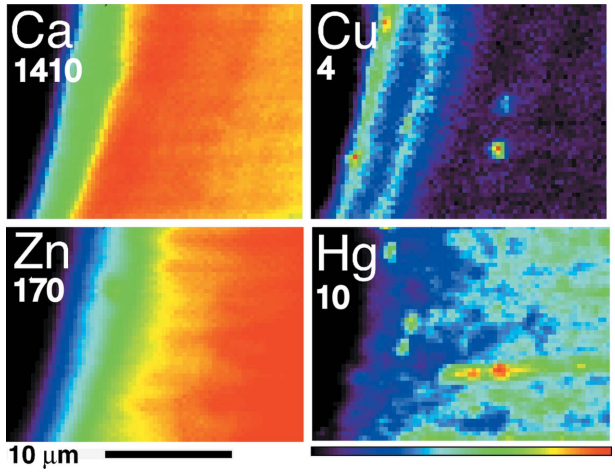

Figure 3
XRF (0.5 μm resolution) elemental distribution maps for a 35 μm × 25 μm region of tooth section indicated by the red box in Fig. 2. Maxima for each element in mg g^{-1} (assuming a tooth density of 2.1 g cm^{-3}) are given below the element symbol.

the sections shown in Fig. 1 are enamel and hence will have a significantly higher density than the dentine on which the calculations are based. Secondly, in Figs. 2 and 3 the left-hand edge of the tooth is closest to the fluorescence detector and hence the escape distance for fluorescent photons is significantly less than that considered in the self-absorption correction calculation leading to an inflated concentration value. It should be noted however that the concentrations shown for the majority of the sections in the figures are within physically reasonable limits for Ca based on the assumption that the dentine is low-density hydroxyapatite (Ten Cate, 1998). In particular, hydroxyapatite, $Ca_{10}(PO_4)_6(OH)_2$, has 399 mg g^{-1} of Ca and, since enamel is ∼97% hydroxyapatite and dentine is ∼70% hydroxyapatite (Ten Cate, 1998), the Ca contents in these regions are expected to be ∼390 and ∼280 mg g^{-1} of Ca, respectively. This is close to the measured values in the XRF maps of ∼320–330 and ∼280–310 mg g^{-1} for enamel and dentine.

4. Discussion

It is clear from Fig. 1 that both Zn and Hg migrate from amalgam fillings and filling linings, through the dentine, and into the pulp of the tooth (subsequently replaced by secondary dentine some time after the filling), which has an active bloodstream. The significant drop in the levels of these metals observed in the secondary dentine that replaced the pulp, as compared with the original dentine, presumably indicates that they were efficiently removed from the pulp *via* the bloodstream before the secondary dentine grew, at which time the Hg was no longer mobile, possibly owing to a change in the chemical state of Hg (see Fig. 2). Localization of Hg in the calculus observed on the edge of the tooth distal to the filling may indicate that Hg is also considerably mobile through the mouth, presumably dissolved by bacterial action in the saliva, or possibly *via* surface diffusion over the tooth surface, and

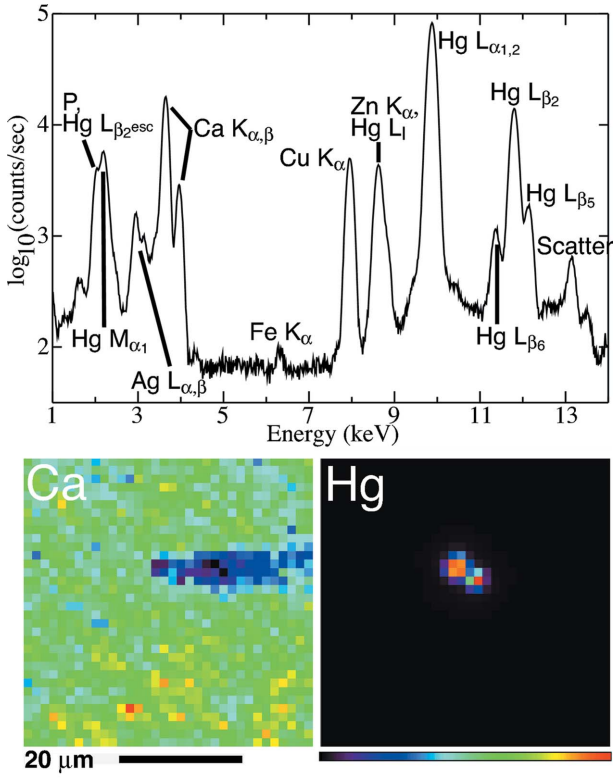

Figure 4
XRF (1.5 μm resolution) elemental distribution maps (below) of a 50 μm × 50 μm region of tooth indicated by the red arrow in Fig. 2, and the XRF spectrum (above, 180 s count time) of the Hg hotspot shown in the XRF map. The peak denoted as P, Hg $L_{\beta2esc}$ arises from a combination of the P K_α emission and a Hg $L_{\beta2}$/Ge escape combination event.

has a higher affinity for deposition in calculus than in other parts of the surface of the tooth. The high concentration of Hg detected in the calculus indicates that particular care should be taken to avoid ingestion of loosened calculus by the patient.

The seemingly anomalous abundant presence of Zn in the dentine considering its low abundance in amalgam is easily explained by the likely use of Zn(II)-based filling lining materials in these teeth. The fact that the concentrations of Zn and Hg in the dentine differ by as much as two orders of magnitude, and that the elemental maps do not follow the same distributions, show that at least part of the mechanisms for the transportation of the two metals through the tooth are quite different. Examination of the elemental distribution maps presented in Fig. 3 provides feasible mechanisms for their transport. The similarity of the Zn and Ca maps, the presence of Zn in the divalent state in the lining, and the smaller ionic radius of Zn(II) (74 pm) *versus* Ca(II) (100 pm) (Shannon, 1976), indicate that chemical replacement of Zn for Ca in the hydroxyapatite structure is the most likely transport mechanism for Zn. Whilst Hg(II) also has ionic radii very similar to Ca(II) of 102 pm (Shannon, 1976), it is initially present only in the elemental state in amalgam. Fig. 3 shows that Hg migrates preferentially through tubules in the dentine along with Cu, suggesting a physically based transport mechanism of malleable Hg-rich amalgam, most likely at the time of restoration. However, analysis of the XANES of Hg in tubules suggests some oxidation of elemental Hg to the divalent state, indicating that a secondary transport mechanism of Hg(II) similar to that for Zn may become important with time. Subsequent association of Hg(II) with sulfides present in the organic contents of the tubules would presumably lead to a reduction in mobility for Hg, and the formation of metal sulfides may also account for the brown staining observed in the optical micrographs.

The cause of the observed inconsistency in the migration of metals across the amalgam/dentine boundary remains uncertain. It is feasible that there is simply inconsistent physical contact over the entire boundary surface; however, the possibility that variation in the exact carious histology (Ten Cate, 1998) on the exposed dentine surface of the cavity affects the migration should also be considered. Unfortunately we were unable to identify distinct histological zones in the dentine of the teeth shown herein.

We attribute the presence of the Hg hotspot in Fig. 4 to the physical transport of Hg-rich viscous amalgam at the time of filling installation into a thin filament of pulp that extended into the region of the filling. Such structures are well known in molars (Berkovitz *et al.*, 1992). Dental amalgam is set in place by incrementally packing a Hg-rich plastic phase into the excavated cavity, with excess viscous Hg removed using a dental vacuum. The physical transport mechanism is supported in this case by the presence of Cu and Ag peaks in the fluorescence spectrum of the hotspot (Fig. 4), as these metals are present in the amalgam. In contrast, a chemical transport process would presumably lead to markedly different distributions of these metals. We believe that the process that we have suggested for the source of the hotspot in Fig. 4 may also lead in particular cases to the direct injection of viscous Hg into the pulp, through a range of structures in the tooth including fractures and larger tubules known to exist between the pulp and crown (Berkovitz *et al.*, 1992).

We are unable at present, with only long-term filled teeth available, to determine any time-dependent data on the migration of these metals through teeth. As such, we are unable to suggest how much Hg may enter the bloodstream on a daily basis but, based on the evidence presented herein, it seems likely that significant amounts do reach the bloodstream, as both elemental Hg and as some form of divalent Hg, *via* at least two different mechanisms of migration through the tooth, as well as ingestion of Hg-rich calculus.

We are grateful for financial support for this work that was provided by Australian Research Council (ARC) Discovery grants (DP0346162 and DP0664706) including an Australian Professorial Fellowship (to PAL), the Australian Synchrotron Research Program (ASRP) grant for the access to APS (PAL and HHH), an ASRP Research Fellowship (to HHH) and an Industry Synchrotron Access Program Grant from the Department of State and Regional Development of the Victorian State Government (HE and PAL). ASRP is funded by the Commonwealth of Australia under the Major National Research Facilities Program. The use of APS facilities was

supported by the US Department of Energy, Basic Energy Sciences, Office of Science, under contract No. W-31-109-Eng-38. We are also grateful for the assistance provided by Dr Cathy Harland.

References

Bates, M. N., Fawcett, J., Garrett, N., Cutress, T. & Kjellstrom, T. (2004). *Int. J. Epidemiol.* **33**, 894–902.
Berkovitz, B. K. B., Holland, G. R. & Moxham, B. J. (1992). *A Colour Atlas and Text of Oral Anatomy, Histology and Embryology*, 2nd ed. London: Wolfe Medical.
Clarkson, T. W., Magos, L. & Myers, G. J. (2003). *N. Engl. J. Med.* **349**, 1731–1737.
Coklica, V., Brudevol, F. & Amdur, B. H. (1969). *Arch. Oral. Biol.* **14**, 451.
EPA (1997). US Environmental Protection Agency, US Government Printing Office, Washington, DC, USA.
Feser, M., Jacobsen, C., Rehak, P. & DeGeronimo, G. (2003). *J. Phys. IV*, **104**, 529–534.
Hoffmann, E., Stephanowitz, H., Ullrich, E., Skole, J., Ludke, C. & Hoffmann, B. (2000). *J. Anal. At. Spectrom.* **15**, 663–667.
Ilinski, P., Lai, B., Cai, Z. H., Yun, W. B., Legnini, D., Talarico, T., Cholewa, M., Webster, L. K., Deacon, G. B., Rainone, S., Phillips, D. R. & Stampfl, A. P. J. (2003). *Cancer Res.* **63**, 1776–1779.
Kingman, A., Albers, J. W., Arezzo, J. C., Garabrant, D. H. & Michalek, J. E. (2005). *Neurotoxicology*, **26**, 241–255.
Kingman, A., Albertini, T. & Brown, L. J. (1998). *J. Dent. Res.* **77**, 461–471.
Reese, R. G. Jr (1997). *Mercury. Minerals Yearbook.* Reston: US Geological Survey.
Sallsten, G., Thoren, J., Barregard, L., Schutz, A. & Skarping, G. (1996). *J. Dent. Res.* **75**, 594–598.
Shannon, R. D. (1976). *Acta Cryst.* A**32**, 751–767.
Ten Cate, A. R. (1998). *Oral Histology: Development, Structure and Function*, 5th ed. St Louis: Mosby.
Van Espen, P. (2002). *Spectrum Evaluation. Handbook of X-ray Spectrometry: Revised and Expanded*, edited by R. Van Grieken and A. Markowicz, p. 29. New York: Marcel Dekker.
Vogt, S. (2003). *J. Phys. IV*, **104**, 635–638.
Vogt, S., Feser, A., Legnini, D., Kirz, J. & Maser, J. (2004). *Synchrotron Radiat. Instrum.* **705**, 1348–1351.
Yun, W., Lai, B., Cai, Z., Maser, J., Legnini, D., Gluskin, E., Chen, Z., Krasnoperova, A. A., Vladimirsky, Y., Cerrina, F., Di Fabrizio, E. & Gentili, M. (1999). *Rev. Sci. Instrum.* **70**, 2238–2241.